Wind resource characteristics and energy yield for micro wind turbines integrated on noise barriers

An experimental study

Chrysochoidis-Antsos, Nikolaos; Amoros, Andrea Vilarasau; van Bussel, Gerard J.W.; Mertens, Sander M.; van Wijk, Ad J.M.

DOI
10.1016/j.jweia.2020.104206

Publication date
2020

Document Version
Final published version

Published in
Journal of Wind Engineering and Industrial Aerodynamics

Citation (APA)
Chrysochoidis-Antsos, N., Amoros, A. V., van Bussel, G. J. W., Mertens, S. M., & van Wijk, A. J. M. (2020). Wind resource characteristics and energy yield for micro wind turbines integrated on noise barriers: An experimental study. *Journal of Wind Engineering and Industrial Aerodynamics*, *203*, Article 104206. https://doi.org/10.1016/j.jweia.2020.104206

Journal of Wind Engineering & Industrial Aerodynamics 203 (2020) 104206

Contents lists available at ScienceDirect

Journal of Wind Engineering & Industrial Aerodynamics

journal homepage: www.elsevier.com/locate/jweia

Wind resource characteristics and energy yield for micro wind turbines integrated on noise barriers – An experimental study

Nikolaos Chrysochoidis-Antsos [a,*], Andrea Vilarasau Amoros [a], Gerard J.W. van Bussel [b], Sander M. Mertens [c], Ad J.M. van Wijk [a]

[a] Process&Energy Department, TU Delft, the Netherlands
[b] Wind Energy Group, TU Delft, the Netherlands
[c] Energy in Transition, The Hague University of Applied Sciences, The Netherlands

ARTICLE INFO

Keywords:
Micro wind turbines
Noise barrier
Field experiment
Urban energy
LCOE

ABSTRACT

This paper assesses wind resource characteristics and energy yield for micro wind turbines integrated on noise barriers. An experimental set-up with sonic anemometers placed on top of the barrier in reference positions is realized. The effect on wind speed magnitude, inflow angle and turbulence intensity is analysed. The annual energy yield of a micro wind turbine is estimated and compared using data from a micro-wind turbine wind tunnel experiment and field data. Electrical energy costs are discussed as well as structural integration cost reduction and the potential energy yield could decrease costs. It was found that instantaneous wind direction towards the barrier and the height of observation play an influential role for the results. Wind speed increases in perpendicular flows while decreases in parallel flow, by +35% down to −20% from the reference. The azimuth of the noise barrier expressed in wind field rotation angles was found to be influential resulted in 50%–130% changes with respect to annual energy yield. A micro wind turbine (0.375 kW) would produce between 100 and 600 kWh annually. Finally, cost analysis with cost reductions due to integration and the energy yield changes due to the barrier, show a LCOE reduction at 60%–90% of the reference value.

1. Introduction

Structural integration of wind turbines with noise barriers could lead to cost reduction and energy yield increase. Potential higher winds on top of the noise barrier might lead to higher wind energy yields. This hypothesis in combination with the strong need for energy yield increase motivated us to investigate further the wind resource properties of this concept through an experimental study for urban wind flows and an energy yield assessment.

This concept exists in patents in China (Luo W. et al. 2016), (Luo W. et al. 2017) and in Korea vertical axis wind turbine integrated with a sound barrier and a velocity sensor (Gi, 2009) as well as with horizontal axis turbines (Changsoo, 2013). Finally, a real world experimentation is on-going near TU Delft in The Netherlands under the same project grant of this publication but the results have not been published yet (PZH, 2018). The safe, reliable and efficient operation of wind turbines in the highly turbulent built environment, where noise barriers are located, is specialised and technically challenging (van Bussel and Mertens, 2005).

Beside this there's also the economically challenging. Micro wind turbines installed within urban environments have low energy payback ratios (Allen et al. 2008), low energy output with low (average of 4%) capacity factors (Encraft, 2009) and the high capital expenditures ranging from 6700 to 10900 €/kW (2017 equivalent from US Dollars) (Orrell et al. 2017) while PV is ranging 2500–6700 €/kW (2017 equivalent from US Dollars) (Fu et al. 2017). All this result to high costs in up to 1.20 €/kWh (Sunderland et al. 2016) while solar can be as low as 0.25€/kWh for the same rated power capacities. This means that small wind costs are somewhere in between 3.5 and 4.5 times higher than PV.

Focussing further out we find that there are 590 km of noise barriers in the Netherlands with potentially suitable foundations for wind turbines (Rijkswaterstaat). Placing 1 turbine every 10 m equals to 59.000 turbines along highway infrastructures. Assuming a 0.375 kW for micro wind turbines (1.5m diameter), like the Dutch-made (WindLeaf), then 17.700 kW of micro-wind turbines could be installed. However, we do not know what the energy yield of these systems will be. This lack of knowledge of how the noise barriers affect the wind flow for micro-wind

* Corresponding author.
E-mail addresses: n.chrysochoidisantsos@tudelft.nl, chrisoconicko@hotmail.com (N. Chrysochoidis-Antsos), G.J.W.vanBussel@tudelft.nl (G.J.W. van Bussel), A.J.M.vanWijk@tudelft.nl (A.J.M. van Wijk).

https://doi.org/10.1016/j.jweia.2020.104206
Received 28 March 2019; Received in revised form 17 April 2020; Accepted 18 April 2020
Available online xxxx

turbine application has led to perform this study. The vision of this study is animated in Fig. 1 below. Finally, in this article we estimate the subsequent change in energy yield for the noise barrier and together with an assumed cost reduction we observe the changes in LCOE.

Relevant literature is presented for wind speed, skewed inflow angle, turbulence intensity and energy yield on top of obstacles which is relevant for the acoustic screens that are investigated in this study. These are non-porous fences, 10 m high, with a gradient of 10°.

1.1. Wind speed

Wind tunnel work of (Raine, 1974) with 0% permeable fences showed speed-up at 1.5H–2H on top of the noise barrier and 1H–4H at the wake of the fence. Wind speed increase is also shown on porous and solid fence experiments in wind tunnel conditions with fence heights ranging (5–16 cm). A wind speed increase of 10–20% between heights of 1.24H and 1.60H and in the leeward direction of the windbreak is shown in (Heisler and Dewalle, 1988) plotting data of (Woodruff N. P. et al. 1959). Wind speed increase ranging from 20 to 50% on top of windscreen for normal flow to the wind screen is shown in wind tunnel validated 3D wind flow simulations behind porous fence (Chen et al. 2012). In (Abohela et al. 2013) increase in wind speed for different types of roofs and directions was found with CFD simulations. Increases ranged from 9.3% to 53%. (Dierickx et al. 2003). identified as well 10% wind speed increase for perpendicular flow to a screen (0.25H leeward from barrier) and at 1.50H on top of it. Finally, (Pena et al. 2016) made an extensive lidar-based analysis of the shelter effects of porous and non-porous effects with subsequent effects on the wind speed.

There is also work that examines flow over ridges, escarpments and other topographic features. Whilst not perfectly analogous, there is a larger focus on the flow above these structures and there are studies that consider the impact of wind direction and the inclination angle. Amplified wind flow from 1 to 1.5 times the upstream velocity was observed in wind tunnel and field tests of (Bowen and Lindley, 1977) for wind flow in the edge of cliffs. In the wind tunnel study of (Rowcroft et al. 2016) up to 20% speed-up was observed on top of a cliff obstacle exposed into yaw angles 0^{o}-40° at locations from 0 to 2H on top of the edge. Turbulence intensity was affected as well. Cliff is a different obstacle to noise barrier spanning 48h downstream, while noise barrier are thin slices of few centimetres. The effect of ruggedness was also assessed in (Rowcroft et al. 2019). Finally, the effects of a cliff on the flow for wind turbine operation are assessed in (Barthelmie and Pryor, 2018), where small speed-up is observed when a flow is perpendicular to the cliff for a turbine placed nearly 3H downstream of the cliff side. Most of obstacles above are not similar to noise barrier in terms of aspect ratio but still is an attempt to utilize similar effects as the ones present in flow acceleration on top of windbreaks (noise barriers).

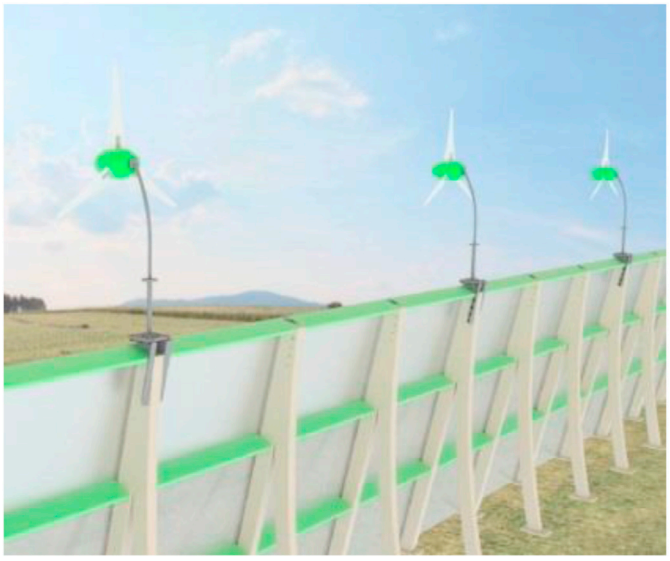

Fig. 1. Visualization of micro wind turbines integrated on a noise barrier.

1.2. Skewed flow angle

Skewed flow angle is the angle from the horizontal and vertical components of wind and is important for the performance of micro wind turbines. (Balduzzi et al. 2012). examined with CFD the effect of skewed flow on vertical and horizontal axis wind turbines on rooftops. For HAWT the skew angle had negative effect while for VAWT positive, for skew angles 0^{0}-40^{0}. (Bastankhah and Porte-Agel, 2016). also examined turbine's performance in yawed flow situations in with theoretical estimation and PIV measurements and found that for yawed flow the power coefficient of the wind turbine is dropping significantly. Finally, (Schreck and Schepers, 2014), observed in experimental data that with skew angle increase, the rotor's C_p (power performance coefficient) is decreasing.

1.3. Turbulence Intensity

Turbulence intensity can affect the energy yield and the performance of the wind turbine. Specifically, (Honrubia et al. 2012) presents the anomalous behaviour of power curve for different turbulence intensities. Power curves vary more when turbulence intensities increase. Also, (Loganathan et al. 2017) concludes that increase of turbulence intensity decreased the power output of a multi-bladed Savonius rotor in an experiment with a constant wind speed of 8 m/s. (Kosasih and Hudin, 2016). observed that the performance of a bare and a diffuser augmented micro wind turbines showed decrease in performance due to turbulence intensity increase. (Cochran, 2002). observed that the kinetic energy at a specific site for small wind turbines can vary by 20% depending on the levels of T.I. In (Kaiser et al. 2004) a theoretical approach shows increase in power in low wind speeds and decrease in power at high wind speeds with high TI and a correction curve is presented only for wind speeds from 7 to 8 m/s. Also from field test in (Rogers and Omer, 2012) author suggests decrease in performance due to turbulence intensity. A Zephyr turbine was used and 20% decreased power was observed with respect to the manufacturer power curve a turbulence levels of 70%.

1.4. Energy yield

In terms of energy yield, (Abohela et al. 2013) found for various roof cases and different wind direction the increase in power for wind energy. In (Kiwata et al. 2011) a higher wind power co-efficient was found for a cross-flow wind turbine integrated above a porous 60% geometric shielding rate windbreak fence examined in a wind tunnel. Finally, as (Drew et al. 2013) agree that urban areas are considered poor sites for micro wind turbine installation and little work has been done for optimizing the placement of the turbines.

We add on prior art with wind time series annual energy yield estimation for a particular noise barrier near Delft and we perform as well a sensitivity analysis by rotating the wind rose in increments.

1.5. Research gap

Several publications exist for wind flows on top of porous and non-porous obstacles and cliffs. However, for noise barriers there is need for real-world dataset with wind properties to be collected and analysed. This will bring more insight on wind energy applications. Our research adds upon the prior knowledge with the addition of results for multiple orientations assessed due to the large dataset given (Chrysochoidis-Antsos, 2019). We emphasize on wind speed on top of the structure and not upstream or downstream. We use as well the skewed inflow angle for estimating the energy yield. The results are translated through a real-world micro wind turbine application into energy yield and cost terms.

1.6. Novelty

The objective of this article is to propose the integration of micro wind turbines with noise barrier structures and assesses its potential benefits in terms of energy yield and cost reduction. The assessment combines an experimental wind resource study results, together with a wind tunnel power performance study in an energy yield sensitivity assessment for micro wind turbine's installed on top of a noise barrier in a single article.

1.7. Outline

The outline of this work started with the literature review in Chapter 1, followed by a detailed description of the set-up in Chapter 2, presentation of Results in Chapter 3, discussion of main outcomes in Chapter 4 and finishes with Conclusions and Recommendations.

2. Set-up description

Two set-ups are realized. An outdoor set-up where all wind flow properties at the noise barrier site are measured and a wind tunnel power curve measurement test. Both explained below.

2.1. Noise barrier set-up

A set-up with 8 anemometers placed on 2 poles on top of the noise barrier and 1 pole as a reference point has been designed and built near a road with a 50 km/h speed limit. The site is on the north side of the ring road that intersects the N470 (regional Dutch road) and the A13 (Dutch National Motorway) as seen in Fig. 3. A dataset of 3-dimensional wind speeds has been collected during the period in 2016–2017 and can be accessed online (Chrysochoidis-Antsos, 2019). 10-minute averaging is used for statistical means. Further, binning methodologies are applied in order to classify the effect of the noise barrier on the wind flow properties per direction of the wind flow relative to the barrier. The documented effects are utilized in a case study for the particular barrier to identify the potential wind turbine energy extracted by the wind turbine model and an LCOE cost change is assessed. For an artistic impression of the wind turbine envisioned, refer to Fig. 1.

2.1.1. Equipment selection

Gill Wind Master 3D sonic anemometers are used to record all wind components. A calibration and measurement validation test was performed for each anemometer, in various angles in all 3 planes (2 horizontal and 1 vertical) as (ISO, 2002) suggests. A correction factor of 1.16 for the vertical velocity component was implemented, as advised by the manufacturer of the sonic anemometers (which was assessed and validated through wind tunnel testing) (Gill Instruments).All results should be treated with the accuracy of the sensors (1.5%RMS at the reference of 12 m/s).

2.1.2. Set-up installation

Dimensions of the set-up and the wind vector reference system are given in Fig. 2. Eight sonic anemometers are installed on 3 measurement poles with brackets. There is a reference pole away from the noise barrier, and two poles behind the noise barrier. All sonic anemometers have cables that guide the signals through underground pipelines to the main electrical cabinet, where the data are recorded.

Some parameters are taken into account for the design of the set-up. These are summarized below:

- The anemometers are placed at distance of 10 times the pole diameter to avoid the **aerodynamical blockage of the cylindrical pole** (Bailey and McDonald 1997). This is also validated by comparing experimental results from various orientations with respect to the position of the bracket.

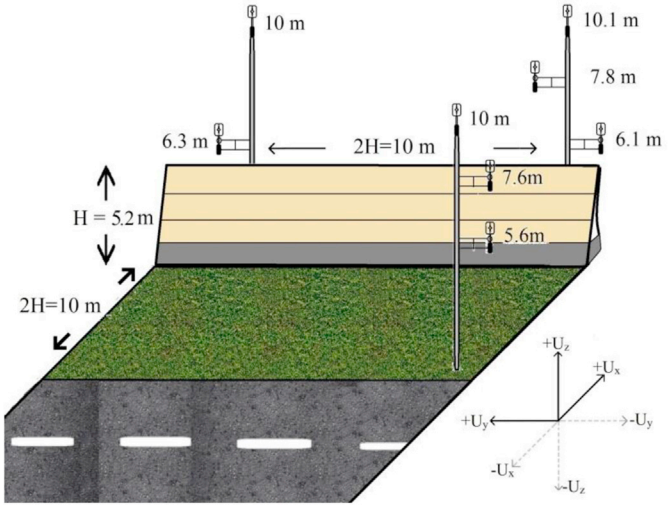

Fig. 2. Schematic of the placement of the poles of the set-up together with the sonic anemometer corresponding heights and the wind speed reference system.

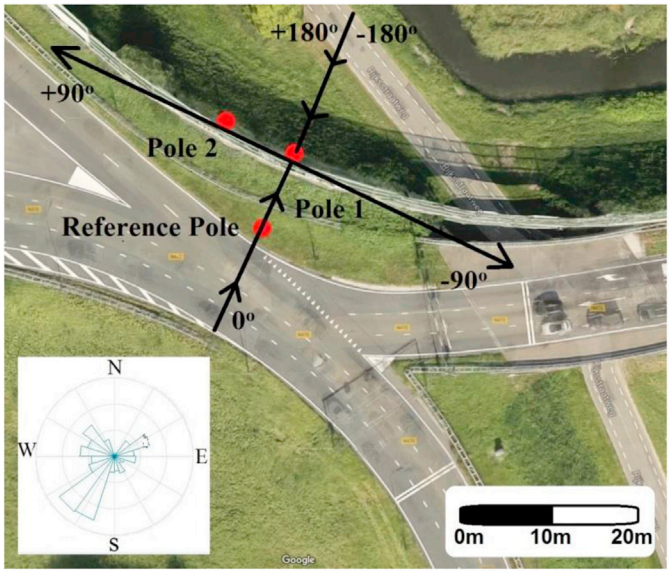

Fig. 3. Top view of the studied noise barrier (bottom left) Wind orientation rose (red circles filled in black) Poles with the sonic anemometers (black lines and arrows) The reference system used in this study. (For interpretation of the references to colour in this figure legend, the reader is referred to the Web version of this article.)

- Poles are fixed in the soil by 1.5m for **structural integrity and avoidance of oscillations** that might affect the measurements from the relative motion of the tower.
- **Passing vehicle effects on wind speed and turbulence** are considered negligible for our set-up, placed on a road passage with a speed limit of 50 km/h. This is 30 km/h less than the experiment in (Eskridge and Rao 1983), with vehicle fleet passing with 80 km/h from a highway. In this they found that for a distance of 15m away from the road a minimal difference in wind speed of 0.1 m/s (at heights of 5 m) and 0.06 m/s (at heights of 10 m).
- **Reference pole is at a distance of 2 times the height of the noise barrier** as seen in Fig. 2 (Wegley *et al.* 1980). suggested that flow is undisturbed in front of small buildings at a distance of 2H. For shelterbelt obstacles such as the noise barrier there are some guidelines but based on empirical assessments. The presence of a road, in Fig. 2,

limited as well the installation of the reference pole more than 2 times the height from the noise barrier.

2.1.3. Wind data characteristics

Data are collected with "WindView" software and processed with MATLAB. During the 13-month period of November 2016 until November 2017, a total of 3066 h were recorded. This is the 32% of all the period resulting in 18396 10-min datasets. The rest was not recorded due to remote connection issues and other limitations. For the recorded datasets, a 10-min median wind direction is used. Only windward datasets are considered and classified (coming from the arc from -90° to 0° to $+90^{\circ}$ in Fig. 3). These datasets are relevant for the study as we examine the effect on windward flow properties. Outliers are removed (circuitry failure, power outages, bird interference and ice formation) to avoid uncertainty on our results. Even if 1 anemometer contained error values then this specific time-series 10-min dataset is excluded. 1.03% of datasets was removed. Finally, the total amount of 10-min periods that are examined is 11.335 (20% of a full year).

2.1.4. Sampling frequency

Data were logged with sampling frequencies of 1Hz (54% of datasets), 2Hz (13% dataset 4Hz (32%of datasets) and 5, 8,16Hz (for the rest 1% of datasets). Even though the selection seems arbitrary in fact it doesn't influence the results. Literature presented that different sampling rates of the same recorded period (10Hz, 4Hz and 1Hz) do not significantly influence the values of turbulence intensity and power spectral density. In particular, changing the sampling rate from 10Hz to 1Hz changed the characteristic turbulence intensity by at most 0.25% of the reference value (Tabrizi et al. 2015). Similarly mean wind speed and inflow angle as well would not be influenced for the purpose of this article which is not to capture turbulent structures of flow, but to use results for micro wind turbine energy yield. We compare 1Hz and 4Hz datasets (~80% of all datasets). Standard deviation of wind speed for sampling frequencies of 1 Hz and 4 Hz can be seen in Fig. 4. This was done for the anemometer placed on the top of the reference pole (see Fig. 2). Sampled points (10-min standard deviation) per wind direction ϕ (^{0}) are less for 4Hz than for 1Hz. But we can make some observations with the help of the grid lines. For wind speeds 0–2 m/s (red dots) and for both datasets with different sampling frequency the standard deviation is between 0 and 1. Same applies for all other wind speed bins where standard deviation is within similar ranges for different sampling frequency datasets. Finally we also present a periodogram (power spectral density) of 4Hz and 1Hz (which was resampled from 4Hz). Again no significant differences are observed. Therefore, all datasets of different sampling frequencies are used in the statistical analysis.

2.1.5. Estimation of wind resource parameters

We compare the data on top of the noise barrier and the data on the reference pole for the reference domain. Wind speed U (m/s), wind direction $\phi(^0)$ and inflow angle $\theta(^0)$ are calculated in each measurement point for each time sample. Input data are the 3 vectors of each anemometer averaged in 10-min periods. Turbulence intensity TI(%) is based on this period. 10-minute averaging is common for wind energy analysis as many handbooks and international standards suggest (Burton et al. 2001). Shorter averaging periods of 5 and 1 min is also used in order to compare the results with the 10 min averaging but as no great deviations were found, they were not considered.

Wind Direction: Results are binned for wind directions. Vector arctangent function is applied for the horizontal wind components U_x(m/s) and U_y (m/s) and the median value of 10-min dataset is selected, thus solving the discontinuity of the degrees (0^0-360^0) (ISO, 2002). Finally we express the wind direction relative to the noise barrier with 0^0 being the perpendicular line as seen in Fig. 3.

2.1.6. Comparison of different pole wind data

Exponential fit is used on 10-min averaged values to estimate wind properties on heights of comparison on the reference pole. For example in Fig. 5 below, the reference anemometer near the road (see Fig. 2 as well) is at a height of 5.6 m while on Pole 1 at 6.1 m. With 3 data points before the noise barrier and exponential fitting we determine the resulting wind speed at the projected height of 6.1 m for the reference pole for the sake of comparison.

2.2. Wind tunnel set-up

Calculation of the wind turbine energy yield is done using an experimentally derived power curve of a commercial downwind micro wind turbine. The experiment was performed in the Open Jet Facility of TU Delft (Low Wind Speed tunnel 0–35 m/s) in Fig. 6. The micro wind turbine is placed in a distance of 3 m from the 2.85 m × 2.85 m nozzle of

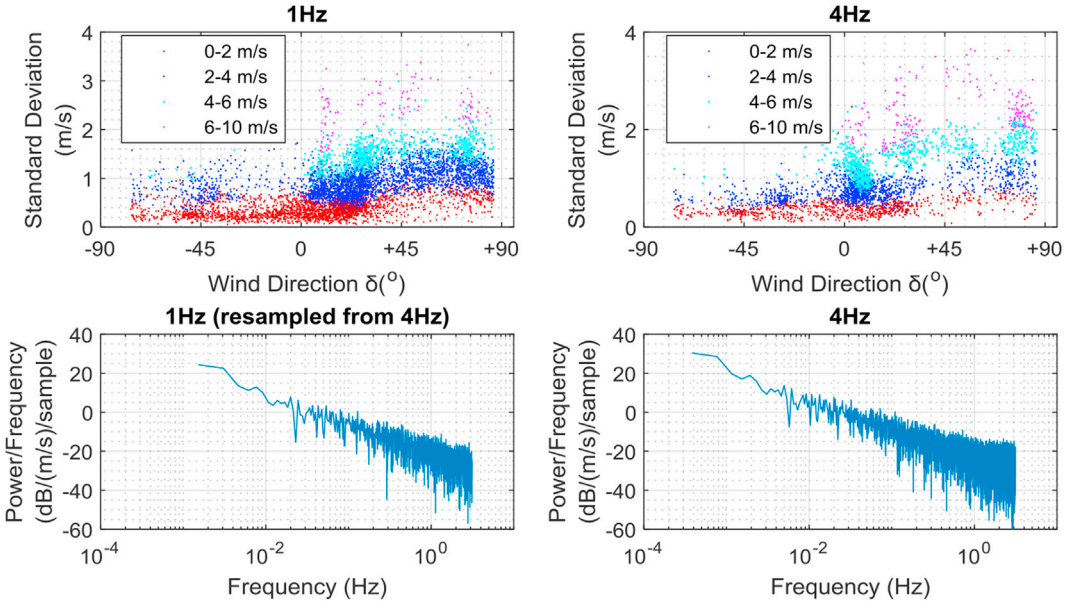

Fig. 4. (top) Scatter plots of the standard deviation σ_u of wind speed for different wind direction and wind speed bins (*see legend)* and different sampling frequencies of 1Hz and 4Hz (bottom) Periodogram of 4Hz and 1Hz dataset (resampled from 4Hz).

Fig. 5. Noise barrier set-up photo from Google Earth.

the wind tunnel, where the control wind speed is calibrated and the blockage effects are corrected (Krynytzky, 1998). Power is recorded with specialised electro-technical equipment (voltage and current measurements) which are further processed in order to derive the power produced (5% error margin). The power fed to the grid is measured including inverter, generator and other losses (IEC, 2005). Fig. 16 indicates the average power values recorded for several wind speeds including the 5% error margin of the sensors. Wind speed sweeps were performed and the average values of Power (W) per wind speed (m/s) are fitted in the curve below. Wind speed is measured with a Pitot-tube placed inside the wind tunnel nozzle and corrected for the distance of the wind turbine from the nozzle.

3. Results

The following chapter presents the equations and the results for all properties assessed.

3.1. Influence of noise barrier on mean wind speed

3.1.1. Methodology

Sonic anemometers provide 3-dimensional wind velocity components. Mathematical equations are applied to estimate the metrics for assessing the wind flow conditions. In our case, U_x (m/s) horizontal wind speed component is perpendicular to the noise barrier, U_y (m/s) horizontal wind speed component is 90° left and U_z (m/s) is the vertical wind speed component (see legend in Figs. 2 and 7).

Wind speed U_{xyz} (m/s) is derived from all the U_x, U_y and U_z components recorded from the sonic anemometers, see Fig. 7. Then these values are averaged with $n_{samples}$, which are the amount of samples within 10-min (depending on sampling frequency).

$$\overline{Uxyz} = \frac{\sum_{i=0}^{i=n_{samples}} \sqrt{U_{x_i}^2 + U_{y_i}^2 + U_{z_i}^2}}{n_{samples}} \quad (1)$$

Wind speed vector magnitudes are used to estimate the speed. Then we compare the wind speed magnitudes at the height h (m) on top of the noise barrier ($Uxyz_{NoiseBarrier}$) with the reference pole at similar height ($Uxyz_{REFERENCE}$). Exponential fitting is used for the sonic anemometers not in the same height of comparison. Wind speed magnitude is used later for energy yield calculations of micro-wind turbine installed on top of the noise barrier. Below is the relative wind speed change $\Delta U_{xyz}(-)$.

$$\Delta U_{xyz}(h) = \frac{Uxyz_{NoiseBarrier}}{Uxyz_{REFERENCE}} \quad (2)$$

3.1.2. Results

A scatter plot of all the 10-min averaged values is shown in Fig. 8 for the sonic anemometer that is right above the noise barrier at 1.17H height (6.1 m from ground). The wind speed bin from 0 to 1.5 m/s has a very large spread. Higher than 1.5 m/s a trend can be observed with wind speed reductions towards −90° and +90° which are parallel wind flow in respect to the barrier. When flow is nearly perpendicular to the noise barrier (−30° until −15°) a maximum increase is observed.

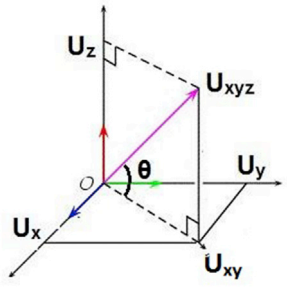

Fig. 7. The 3 components of wind speeds (m/s) U_x, U_y and U_z. The horizontal wind vector U_{xy} and the U_{xyz} resultant vector for the magnitude of wind speed together with the inflow angle θ(°).

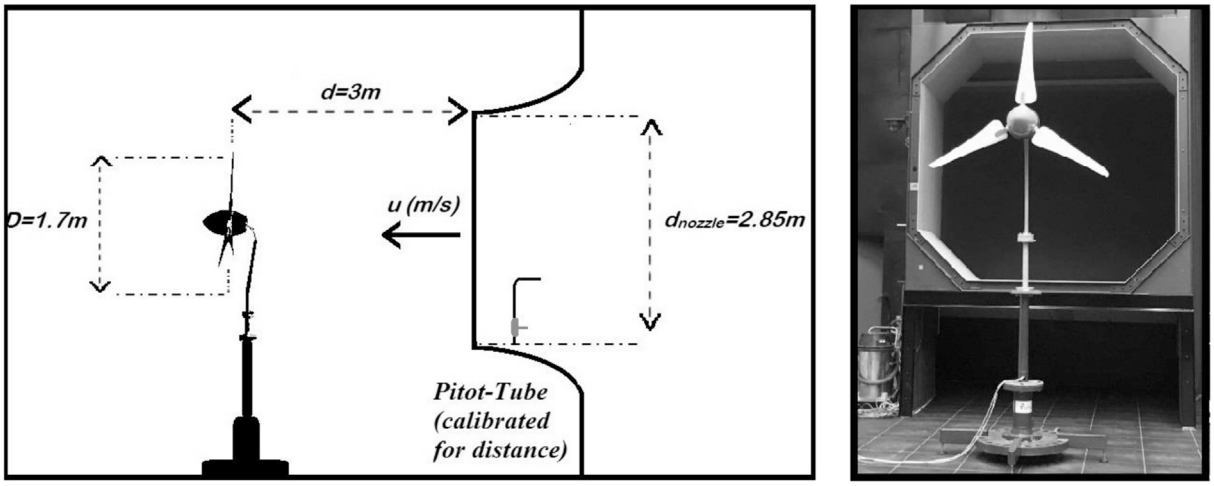

Fig. 6. (Right) Micro wind turbine placed in front of the nozzle of Open Jet Facility in TU Delft (left) plan drawing of the distances.

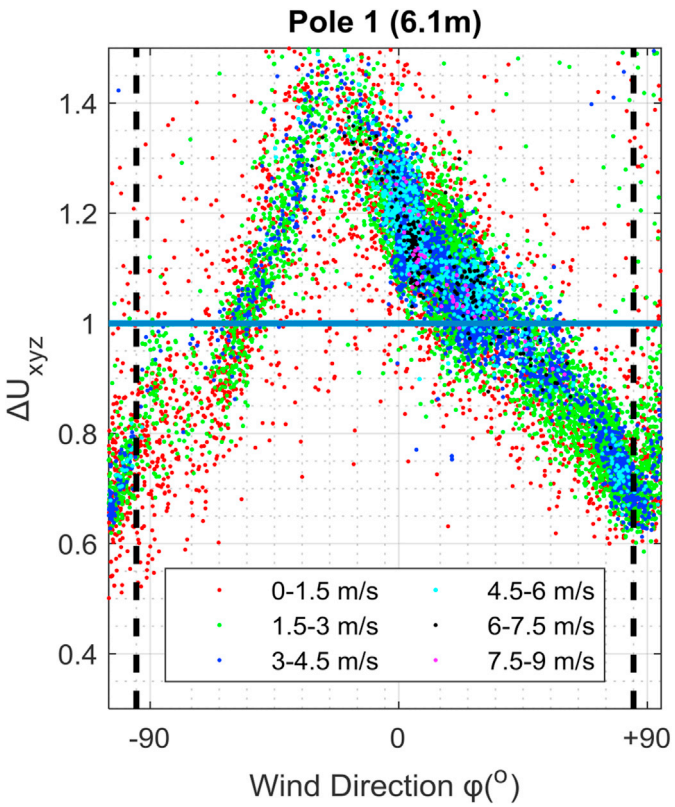

Fig. 8. Scatter plot of wind speed relative change (ΔU_{xyz}) for the sonic anemometer places at 1.17H (Pole 1 at 6.1 m) on top of the noise barrier. All coloured dots represent different wind speed bins (*see legend)* with 0° being perpendicular.

In Fig. 9, we plot as well the wind speed differences for different heights. The data are categorized for 10° increments from −90° until +90°, which is the windward side of the barrier. The most positive increase is observed in perpendicular flows (−30° until 0°) while is decreases in parallel flows in the edges of the graphs. The right part of both graphs is less steep while the left part is steeper, this might be attributed to the localized terrain.

The positive change is higher rather than negative with maximum of 1.35 (−20°) and minimum of 0.75 (+80°).In Fig. 9 we observe that the maximum changes do not occur in a perfectly perpendicular flow at 0° but at −20°. Similarly at +20° there are no changes (ΔU_{xyz}~0), but as we move more parallel then a wind speed reduction is observed for both sides. These lead to recheck the calibration and positioning of the sensing equipment as well as the methods to assess the orientation of the barrier but no abnormalities were found. Therefore, a hypothesis is made that pressure reduction due to the presence of the bridge shown in Fig. 3 (at direction −40° until −10°) might lead to this shift of the localized maxima. Results of Fig. 9 for the wind direction of 0° match well the references presented in Chapter 1, where most authors observed increases from 5% to 35% in wind speed on top of windbreaks.

3.2. Influence of the noise barrier on inflow angle

3.2.1. Methodology

Inflow angle θ(°) is used to estimate the wind turbine's rotor flow misalignment losses. The $\theta_i(^0)$ inflow angle for the time step(i) is calculated using the resultant vector of the horizontal wind components U_x and U_y and the vertical wind component U_z with the arc tangent function. When every angle is estimated for the 10-min period then an averaging is performed.

$$U_{xy_i} = \sqrt{U_{x_i}^2 + U_{y_i}^2} \tag{3}$$

$$\theta_i = \arctan\left(\frac{U_{z_i}}{U_{xy_i}}\right) \tag{4}$$

Several studies have been conducted that investigate the flow misalignment effects (mostly from yaw misalignment) in loads, power performance just like in (Schulz et al. 2017) where it is found that power losses can be as much as 30% at 30^0 misalignment. Therefore, inflow angle describes the flow misalignment of a potential installed rotor on top of the barrier and it used to estimate the affected energy yield. Micro wind turbines have usually a tip vane or at designed to self-align with the flow in order to minimize the yaw misalignment losses but when the inflow angle varies in the vertical component there is not such a mechanism to allow the rotor to align. Thereby we estimate this component in order to derive the losses resulting from the inflow angle θ^o as in Fig. 10. The energy yield is further estimated with the magnitude of the U_{xyz} (m/s) and the effect of inflow angle $\theta(^0)$ as a misalignment loss.

3.2.2. Results

Inflow angle $\theta(^0)$ when skewed affects the power performance of the micro wind turbine. Fig. 11 presents a time series of 2 s (4Hz sampling) of the flow field between the reference pole and Pole 1. (Kiya and Sasaki, 1983). and (Largeau and Moriniere, 2007) have visualized the effects on wind flow in front of wall structures with an emphasis as well on the periodic swell and shed in front of the noise barrier as well as the separation bubble behind the noise barrier. Our intention is different as we present only data at the installation height of micro wind turbines and do not focus on more specific flow properties related to turbulence behaviour studies.

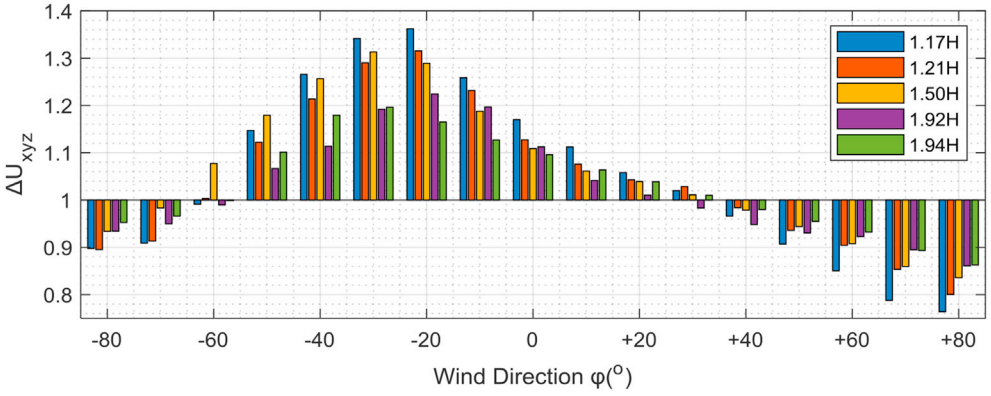

Fig. 9. Bar plot of wind speed relative changes for different directions and heights for the reference arc (-90^0 until +90°) with 0° being perpendicular.

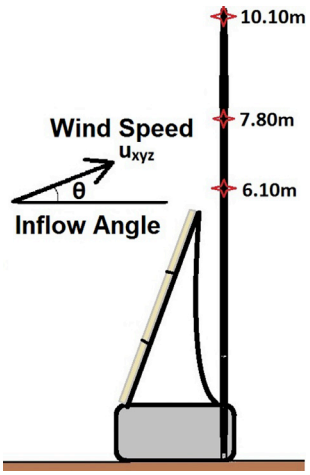

Fig. 10. Wind speed U_{xyz}(m/s) magnitude vector and the inflow angle $\theta(^0)$, illustrated for a perpendicular flow indicating the presence of sonic anemometers with red stars in different heights for Pole 1. (For interpretation of the references to colour in this figure legend, the reader is referred to the Web version of this article.)

Contour and arrows are constructed using 6 points (Reference Pole and Pole 1 anemometer height locations in Fig. 3). First, vertical exponential fit is performed for the wind shear and second a horizontal fit between poles. Blue towards yellow contour on the back represents instantaneous wind speed U_{xyz}(m/s). Black arrows overlaid represent inflow angle. The representation is questionably oversimplified and neglects many wind flow phenomena happening between the 2 poles such as vortexes, especially in front of the noise barrier. It simply illustrates the averaged flow parameters. In particular, wind speeds increase (blue contour becomes yellow) in perpendicular wind directions to the barrier ($\phi = -5^\circ$ until $\phi = 10^0$). Inflow angles θ (black arrows) have a tendency to move upwards and surpass the barrier thus high inflow angles. Finally, the variability of wind speed and the stochastic nature of wind can be seen in these time series.

Large variations in inflow angle mean more variations in power due to the more frequent misalignment of the rotor with the skewed flow leading to lower aerodynamical performance coming from the reduction of the $\cos^3\theta$ rule (Manwell et al. 2009). Therefore it is worthwhile presenting the standard deviation of the inflow angle presented in Fig. 12.

Standard deviation of inflow angle $\theta(^0)$ increases at the edges of the box plots for Pole 1 which represents the parallel to the barrier flows. Also in perpendicular flows (near 0°) we observe decrease of the standard deviation for Pole 1 comparing with the Reference Pole for all heights. Boxes represent the values in between the 25th and 75th percentile of each data bin. The line in between the boxplot is the median value. The whiskers include all values that are in between 1.5 times the interquartile range, while the outliers are plotted using a spatial randomization with Jitter function for better visuals.

Fig. 13 presents the 10-min averaged inflow angle for 3 heights h(m) and different wind direction $\phi(^0)$ bins. For 1.17H a maximum of 22^0 is observed at −15° wind direction. For 1.50H inflow angle has a maximum of 17° and for 1.94H it is 8°. This result could be compared with the wind tunnel experiment and CFD study (Hagler et al. 2011) which similarly showed increase in inflow angle on the tip of the barrier. A trend is observed that in parallel flow (close to −90° and +90°) inflow angle decreases and especially near the −90° region. Due to this drop we comment that the terrain next to the installed poles as in Fig. 3 and the complex road topology with a small bridge and an air-hang noise barrier segment might be factors of lower wind angles present for both poles above the barrier, similarly as with the shift of localized maxima for wind speed.

3.3. Influence on turbulence intensity

3.3.1. Methodology

Turbulence intensity TI_{xyz} (%) of the U_{xyz} (m/s) magnitude is determined using the ratio of the 10 min average mean magnitude of U_{xyz}(m/s) and the Standard Deviation σ_{uxyz}(m/s) of each 10-min dataset:

$$T.I._{U_{xyz}} = \frac{\sigma_{Uxyz}}{U_{xyz}} \quad (5)$$

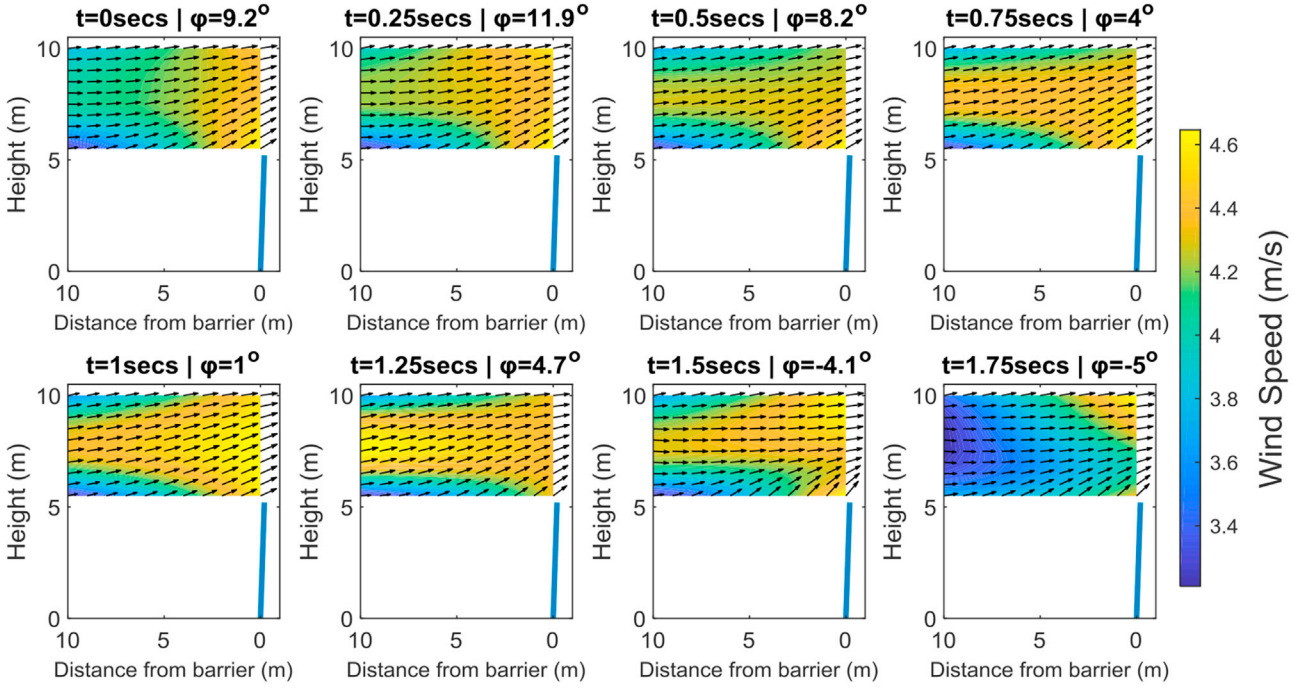

Fig. 11. Time series (2 s – 4Hz) of wind field contour (blue-yellow) and quiver plot (black arrows) for the noise barrier near-perpendicular flows ϕ=(-5^0+10^0). Distance from barrier is 0 at reference and 10 on top of the barrier. (For interpretation of the references to colour in this figure legend, the reader is referred to the Web version of this article.)

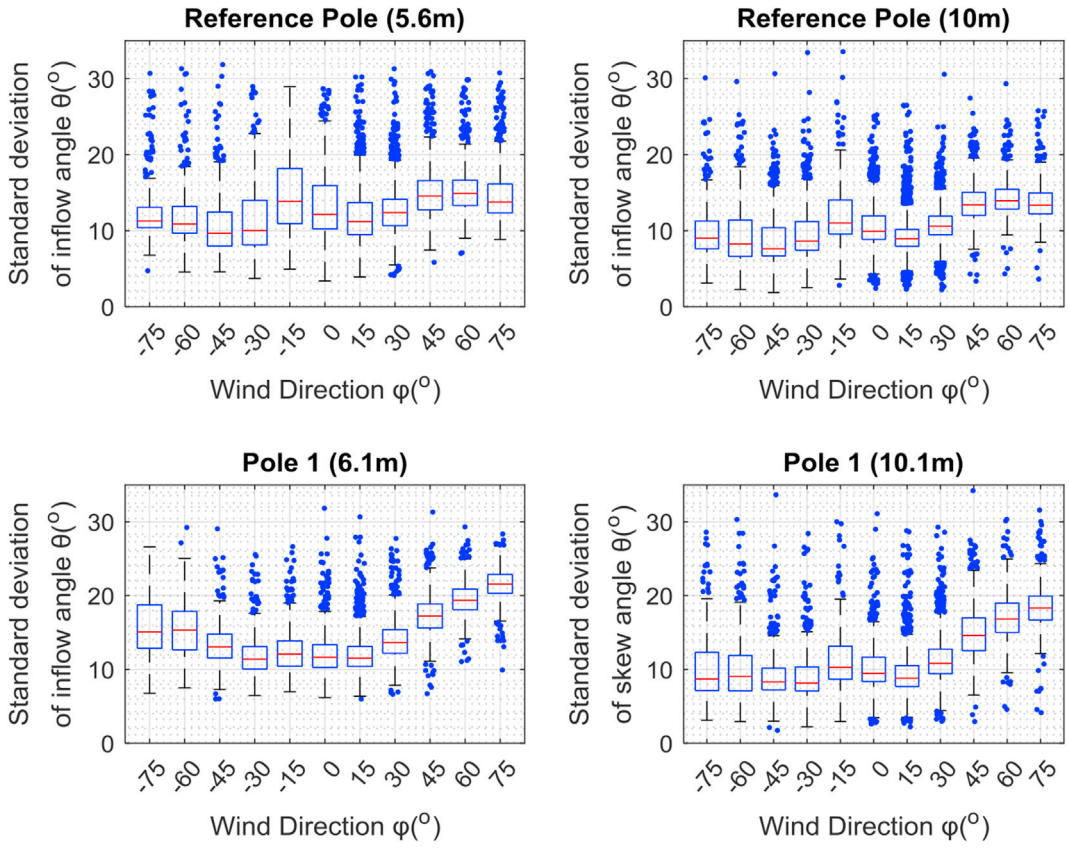

Fig. 12. Box plots indicating the 10-min standard deviation of the skewed inflow angle $\theta(^0)$ for the sonic anemometers placed (top) on the reference pole (bottom) and noise barrier at pole 2 at different heights.

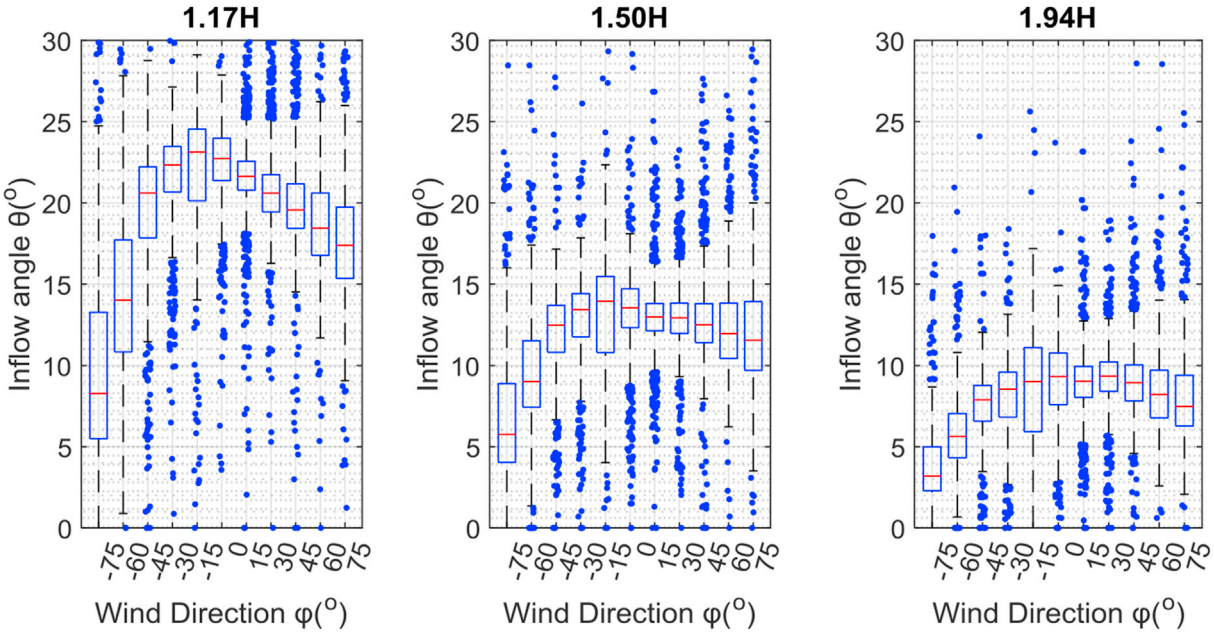

Fig. 13. Box plots of 3 different heights of the 10-min averaged inflow angle $\theta(^0)$ for different wind directions $\phi(^0)$.

3.3.2. Results

In Fig. 14 we present a comparison of turbulence intensity of 2 sonic anemometers. It ranges between 20 and 40% for perpendicular (-30^0 until $+15^0$) and 40–60% for parallel flows (-75° until -60° and $+60^\circ$ until $+75^\circ$). Spread of TI is greater for wind speeds (<2 m/s). Box plots are used and their property interpretation is found in chapter 3.1.2. Parallel flows at the tip of the noise barrier exhibit increases in turbulence intensities. Flow mixing on top of the barrier might lead into more turbulent flow structures. Decrease of turbulence intensity happens in

perpendicular flows. A hypothesis is that large pressure difference before and after the noise barrier leads to increased wind mass flow (thus increase in wind speed) and thereby decreases the turbulence intensity as its value depends on the average mean wind speed on the denominator.

As discussed in chapter 1, turbulence might lead to power variations. Positive effect of high turbulence could occur in lower wind speeds, leading to greater power and more chances for the rotor to continue idling thus increasing the chances of reconnecting and generating useful power. Turbulence intensity is a factor to take into account as urban environment wind speeds tend to be rather low. However, we do not use it in the energy yield estimation as more detailed modelling approach would be required to correct the power performance of the wind turbine for certain ranges of turbulence intensity.

3.4. Annual energy production sensitivity analysis and results

Literature identifies wind resource assessment as very important as current tools could overestimate the energy yield of wind turbines (Drew et al. 2013). We perform a sensitivity analysis for the wind turbine yield and use the corrections from the results of the assessment on wind speed and inflow angles for the energy yield.

3.4.1. Sensitivity analysis parameters

We estimate Annual Energy Production (AEP) in kWh for 3 different heights above the noise barrier (1.94H, 1.55H and 1.17H) based on the heights of the anemometers on Pole 1. We also rotate the annual time series wind rose in steps of 20° for a full 360^0 rotation by keeping the noise barrier still as in Fig. 15, where $\delta(^0)$ is the rotation angle that is applied in each time step of the annual time series. Therefore, for each wind field rotation angle $\delta(^0)$only the relative wind direction $\phi_i(^0)$ with respect to the noise barrier would change and the effects on the total Annual Energy Production are estimated.

3.4.2. Methodology

The baseline Annual Energy Production (AEP) of a micro wind turbine on top of the noise barrier is calculated with a 12-month 10-min wind speed and direction record from Rotterdam Airport (KNMI, 2015). Sensitivity could have been assessed by using more annual datasets but we limited the paper due to size constraints to 1-year. Wind speed correction is applied for the differences in surface roughness between the two locations, resulting in wind time series at the reference pole U_i (m/s). Another correction for effects of the noise barrier on wind speed and inflow angle is used. Finally through a look up table we find the energy yield of a reference micro wind turbine (375Watts) for each time step that corresponds to the corrected wind speed. Energy yield of the wind turbine is based on wind tunnel measured power curve. Wake losses are excluded as we evaluate the performance of a single turbine rather many installed on top of noise barriers. Finally, we sum all time steps to derive the Annual Energy Yield (AEP) in kWh.

The annual free stream energy yield, AEP_0 (kWh) at a height h(m) from ground is without the influence of noise barrier and is used as a reference for comparison. The corrected wind speed U_i(m/s) at the height h(m) of turbine installation is used.

$$AEP_0\left(h\right) = \sum_{52560}^{i=1} E_i(U_i\left(h\right)) \tag{6}$$

The AEP(kWh) is then corrected for speed-up associated effects from the noise barrier. We apply the wind speed factor ΔU_{xyz} (−) from chapter 3.1.2. This varies as a function of the relative wind direction $\phi_i(^0)$ and is applied to the wind speed U_i(m/s). The resulting annual energy yield is AEP_1(kWh), which includes noise barrier wind speed magnitude ΔU_{xyz} effects and assumes an aligned rotor with the skewed incoming flow on top of the noise barrier. In reality this is not true, but with this variable we can isolate the effects due to skewed angle flow misalignment and the relative change in wind speed due to the noise barrier. AEP_1(kWh) is estimated for different heights h(m) and different wind field rotation angles $\delta(^0)$ as part of the sensitivity analysis.

$$AEP_1(h,\delta) = \sum_{52560}^{i=1} E_i\left(\Delta U_{xyz}(h,\delta,\phi_i)\cdot U_i\right) \tag{7}$$

Finally, AEP_2 (kWh) contains the additional correction for

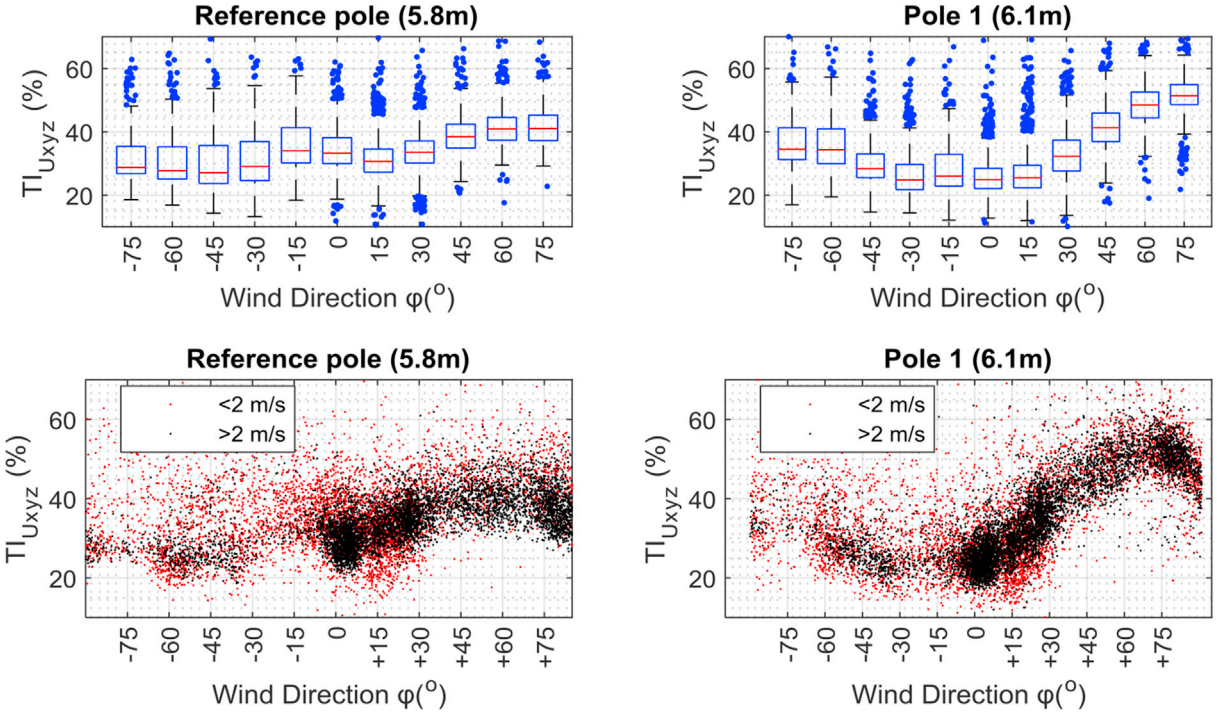

Fig. 14. Box plots of the turbulence intensity TI(−) of the lowest sonic anemometers (5.8m and 6.1m) for the reference pole and the noise barrier (Pole 1) (box area is 25th and 75th percentile).

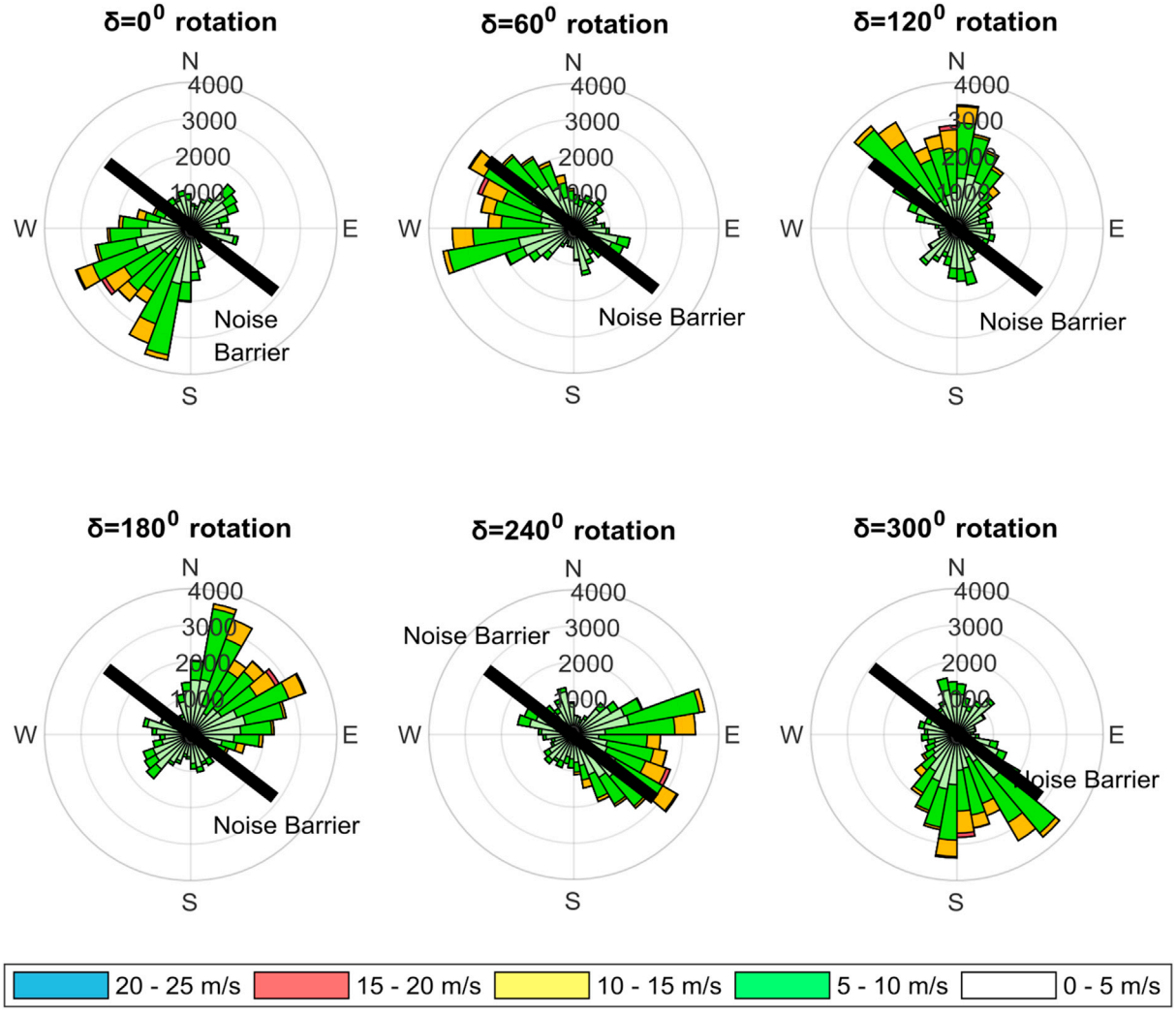

Fig. 15. Binned wind speed rose rotation by angle δ (clockwise) for the sensitivity analysis. Black line indicates the noise barrier. Legend indicates the wind speed bins.

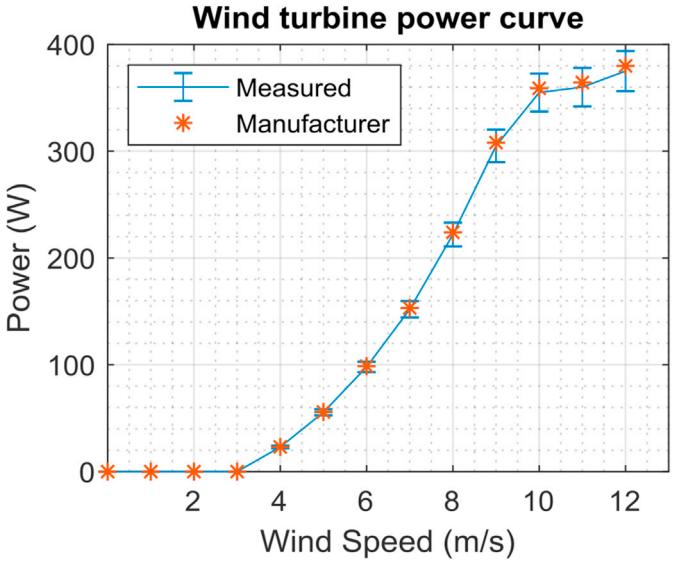

Fig. 16. Power curve of the WindChallenge micro wind turbine recorded in the OJF wind tunnel experiment and compared with manufacturer's.

misalignment losses due to the skewed inflow angle. This is done applying the $\cos^3\theta$ correction at each time step. This is mostly used for yaw misalignment (Manwell et al. 2009) but in our case we apply it for the skewed flow misalignment.(Ciri et al. 2018). found $\cos^3\theta$ as a good approximation for normalized power but it slightly underestimates power while the $\cos^2\theta$ theory slightly overestimates power. In our approach we use the more conservative yaw correction $\cos^3\theta$ law. AEP_2 (kWh) is estimated for different heights h(m) and different wind field rotation angles $\delta(^0)$ as part of the sensitivity analysis.

$$AEP_2\left(h,\delta\right)=\sum_{52560}^{i=1}E_i\left(\Delta U_{xyz}\left(h,\delta,\phi_i\right)\cdot U_i\right)\cdot\cos^3\theta_i\Big) \tag{8}$$

The relative impact on AEP of speed-up associated with the noise barrier can be expressed as: $\eta_{aligned}$ (−), which is the ratio that describes the influence of the noise barrier to the wind speed vector magnitude expressed in energy terms.

$$\eta_{aligned}(h,\delta)=\frac{AEP_1(h,\delta)}{AEP_0(h)} \tag{9}$$

Similarly the relative impact of flow misalignment due to the inflow angle is expressed as: $\eta_{misaligned}$ (−), which is the ratio of that describes us the losses in energy due to the misalignment of the rotor with the incoming skewed flow.

$$\eta_{misaligned}(h,\delta) = \frac{AEP_2(h,\delta)}{AEP_1(h,\delta)} \tag{10}$$

Finally, the overall impact on AEP is expressed as: $\eta_{nbtotal}$ (−), which is the ratio that describes the total influence of the noise barrier, taking into account both the influence to the wind speed but also accounting for the skewed flow misalignment effects. See equation (11) below as well as equation (12).

$$\eta_{nbtotal}(h,\delta) = \frac{AEP_2(h,\delta)}{AEP_0(h)} \tag{11}$$

$$\eta_{nbtotal} = \eta_{aligned} \times \eta_{misaligned} \tag{12}$$

In order to derive all above mentioned variables we used the following:

Power curve: Below you can see the measured power curve in the wind tunnel and the validation with the manufacturer's data. Whiskers indicate error margins of the sensor equipment and different measurements performed. Power curve is used as a look-up table for the Annual Energy Production (AEP) estimations.

Wind speed corrections: Corrections are applied based on local roughness (the site is 3 km away from the weather station) in order to translate it for the noise barrier case before applying corrections for the noise barrier. First we translate the weather station time series wind speed of time step i to a blending height and then we translate to the height of the reference pole.

- The wind speed dataset from the airport is translated to a blending height of 60 m with log wind law. Local roughness parameters are being taken into account. Rotterdam airport weather station is placed on flat terrain area without presence of obstacles and therefore the roughness length is assumed to be 0.03 (WMO, 2010) while zero-displacement is 0. Blending height h_2 (60m) and weather station height h_1 (10m) are used.

- Wind speed at blending height is then translated to the three hub heights of Pole 1 at the noise barrier. Table 1 presents zero-displacement height d and roughness length z_o which have been determined with an empirical approach from wind gradient data of the reference pole for the windward side in Fig. 3. For the downwind side of the barrier as seen in Fig. 3 they were determined by the elevation, the terrain and the surrounding landscapes taking into account the (WMO, 2010) classifications because of lack of reference data from measurements.

$$U_i = U_{ref} \times \frac{\ln\left(\frac{h_2-d}{z_0}\right)}{\ln\left(\frac{h_1-d}{z_0}\right)} \tag{13}$$

Noise barrier correction factors: Corrections on wind speed due to noise barrier are applied based on results in Fig. 9. Wind speed is multiplied at each time step with ΔU_{xyz} for the corresponding relative wind direction ϕ_i with the barrier which depends on the wind direction from the dataset used (KNMI, 2015). Effects for the downwind side of the noise barrier (symmetry) are "mirrored" since we recorded the effects only from the upwind side of the barrier. Despite the fact that it is a questionable assumption because the noise barrier is not erected vertically but with a given angle to the vertical, it had to be assumed because experimental data are only available for 1 side of the barrier. Thereby, we assume the same effects on the other 180^0 arc behind the barrier. For example, in Fig. 3 if at a certain time step wind comes from +100° then we mirror the effect and use the correction factors from results that apply for +80°. Similarly, from −150° we correct with results from −30°. The correction factors used are the ΔU_{xyz} (ϕ_i) for wind speed used for AEP_1 and AEP_2 and the $\theta(\phi_i)$ for skew corrections in AEP_2. Finally, each relative wind direction ϕ_i is corrected with respect to the wind field rotation angle $\delta(^0)$ because the wind direction relative to the noise barrier for each rotation would change according to the rotation angle and thereby the effects on wind speed would change accordingly.

Table 1
Surface parameters of the study area as a function of wind direction sector. Empirical data from −90° until +90°.For data with asterisk * (WMO, 2010) classification used.

Sector(°)	d(m)	z_o(m)
(-180°)to(-150°)*	2.30	0.20
(-150°)to(-120°)*	2.00	0.19
(-120°)to(-90°)*	2.60	0.26
(-90°)to(-60°)	3.00	0.75
(-60°)to(-30°)	2.00	0.16
(-30°)to(0°)	3.10	0.09
(0°)to(+30°)	3.00	0.08
(+30°)to(+60°)	2.30	0.22
(+60°)to(+90°)	1.70	0.15
(+90°)to(+120°)*	1.90	0.18
(+120°)to(+150°)*	2.00	0.20
(+150°)to(+180°)*	2.20	0.18

3.4.3. Results

Energy yields in top graph of Fig. 17 show the sensitivity of energy output of a wind turbine on top of a barrier for wind field (wind and direction dataset) rotations of 20° including the noise barrier effects. The misaligned energy yield (AEP_2) are always lower as they contain effects on wind speed magnitude and inflow angle. For the aligned energy yield (AEP_1), the effects only on wind speed magnitude are considered assuming that the rotor is always pointing at the resultant wind vector. Annual energy production at 1.94H ranges from 400 to 600 kWh with some localized maximum and minimum points which depend on orientation of the noise barrier (projected from the wind field rotation). For 1.50H installation height, energy ranges from 300 to 550 kWh and for 1.17H ranges at 150–430 kWh. Installing the turbine closer to the barrier has more uncertainty as the ranges are more widespread. Total annual energy production is very sensitive to relative noise barrier rotation angle with the wind rose. In Fig. 17 bottom graph, annual energy production is compared with the straight line (reference yield). Positive effect is mostly observed but there are cases with significant drop in energy yield (40°, 60°, 80°, 140°, 220°, 260° and 280°). Importance of site assessment is shown between 120° and 160°, where only for a range of 40^0 we observe a difference from 600 kWh to 400 kWh.

In Fig. 18 we explain the dominant effect on wind energy yields for each noise barrier orientation. The $\eta_{nbtotal}$(%) is mainly affected by the wind speed magnitude changes as seen in the left graph with $\eta_{aligned}$(%) while the flow misalignment $\eta_{misaligned}$(%) always contributes in a negative way but to a less extent. In particular, for the effect of the wind speed magnitude and especially for installation heights of 1.17H, the energy yield could range from 60% to 150% of the reference total annual energy yield. For 1.50H, the ranges are 75%–140% and for 1.94H, the ranges are 85%–120%. The effect of inflow angle leading to a misaligned rotor to the flow in middle graph of Fig. 18 increases closer to the barrier as the inflow angle increases. But overall it influences energy yield to a less extent with respect to the wind speed magnitude changes. For 1.94H, the total energy yield is ~97% of the reference yield while for 1.75H is ~92% and for 1.55H is ~83%. Finally, the total energy yield with all the noise barrier related effects is compared with the free stream wind turbine energy yield. This is presented with the $\eta_{nbtotal}$ (%) in Fig. 18. The lowest position at 1.17H noise barrier height is the less profitable attributed mainly to the flow misalignment losses. The other 2 height locations are either marginally positive or negative with ranges from 90% to 120%. For the increments from 250^0-300^0 the performance is greatly and negatively affected at 30–60% of the free-stream energy.

We conclude from the results that noise barrier can have both negative and positive influence on energy yield depending on its orientation

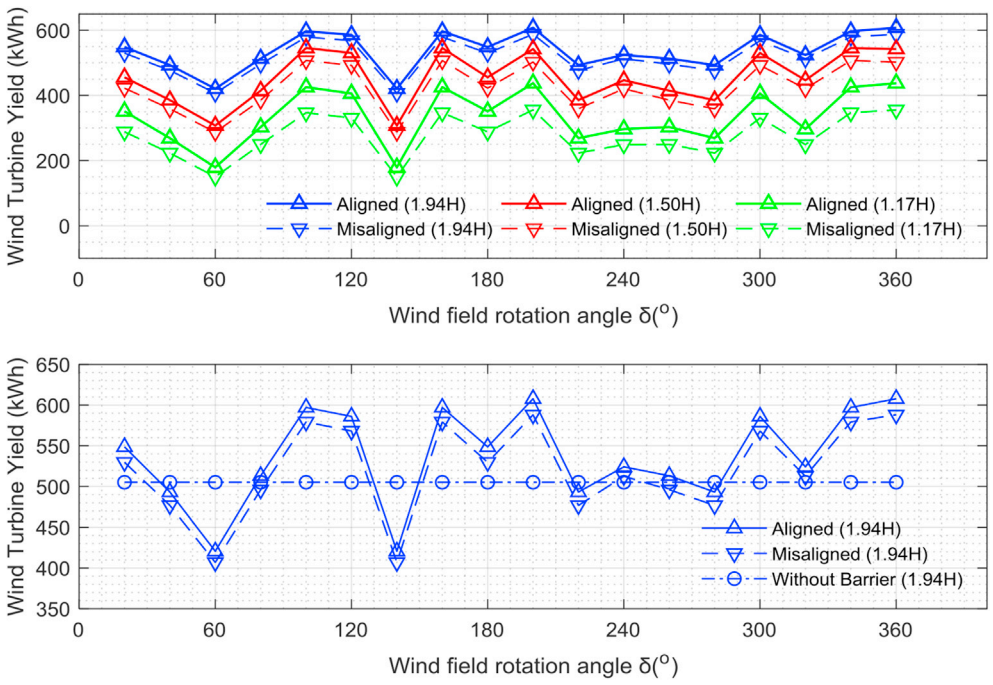

Fig. 17. (top graph) Sensitivity analysis of total annual wind turbine yield for an aligned and misaligned flow towards a micro wind turbine installed on top of a noise barrier at different heights and for 20° increments of wind field rotation (bottom graph) Without Barrier, aligned and misaligned flow total annual wind turbine yields for 20° increments of wind field rotation.

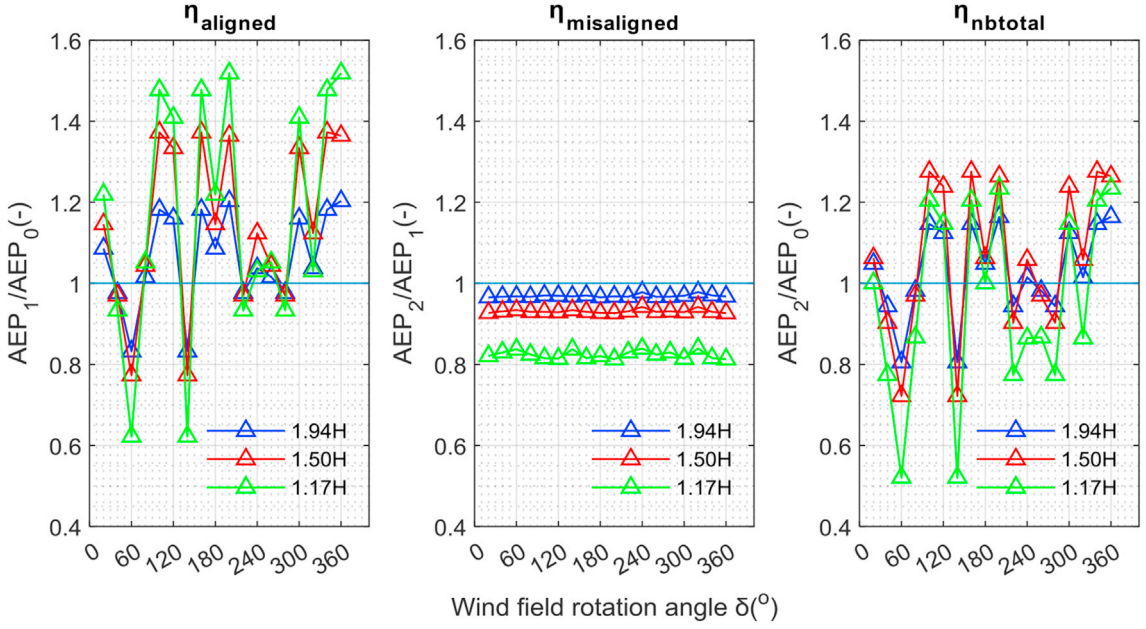

Fig. 18. (Left) Change in annual energy yield (AEP) on top of the noise barrier as a function of the wind field rotation angle $\delta(^0)$ (left) not taking into account skewed inflow angle $\theta(^0)$. (middle) due to the skewed flow misalignment taking as a reference the energy yield of the aligned flow (right) taking into account both effects.

to the wind field. Installers should be very careful designing such systems, paying great attention to the wind resource assessment and energy yield estimation including noise barrier effects.

Finally Table 2 summarizes the results for the reference case of the existing noise barrier:

In Table 2, the influence of the noise barrier in the total annual wind turbine yield for all heights 1.17H, 1.50H and 1.94H is positive. We can observe respectively an overall increase of 22%, 25% and 20% for these heights. Increase due to wind speed magnitude is greater than these numbers but the skewed flow misalignment with the micro wind turbine rotor leads to a slight decrease by 80%, 92% and 96% of the yield that was estimated taking into account only the wind speed magnitude increases. This case is positive but in a different noise barrier orientation with the same wind field there is possibility for negative influence of the energy yield as the case of 60° wind field rotation with the turbine producing 50%, 70% and 80% of the reference.

4. Discussion

Here we discuss relevant situation where the results are relevant and

Table 2
Case study for the current noise barrier orientation.

Case study of the current noise barrier (corresponding to wind field rotation angle 360°)			
	1.17H	1.50H	1.94H
Total annual energy yield without noise barrier effects (kWh)	290	395	505
η_{align} (−)	1.51	1.36	1.20
$\eta_{misaligned}$ (−)	0.81	0.92	0.96
$\eta_{nbtotal}$ (−)	1.22	1.25	1.15
Noise barrier Influenced Yield (kWh)	354	494	580

we discuss about the economics of micro wind turbines on noise barrier with respect to the results.

4.1. Wind resource characteristics

Some noise barriers are placed in complex topologies near highways, with elevated roundabout and other elements. (Lubitz and White, 2007). studied effects of such hills in wind tunnel and found that wind speeds increase when flows are perpendicular to the ridge of hills. However, expansion of wind resource assessment to cover those cases as well is needed. Finally, regarding local wind flow characteristics, the shift in localized maxima (probably explained by the presence of the bridge) intrigues us to suggest further wind tunnel validation along with numerical modelling and CFD calculations in order to derive a concrete model for relevant flows.

Designing turbines in different way might alleviate skewed inflow angle effects. For example, predefined wind turbine hub angles could alleviate these losses. But new loading types will start affecting the operation of the turbine (e.g. gravitational). Results in Fig. 13 showed that the turbine on top of the noise barrier would be mostly exposed to skewed flow between 5^{o}-25°. As horizontal axis wind turbines underperform in skewed flow and vertical axis wind turbines seem to have better power performance coefficient (Balduzzi et al. 2012). We could make a hypothesis that there is potential for further energy yield increase with vertical axis wind turbines.

Turbulence intensity (TI) decreases for perpendicular flows while wind speeds increase and vice-versa TI decreases for parallel flows while wind speeds tend to decrease. Literature suggests that increased turbulence intensity might lead to more energy production for low wind speed ranges of near ground applications and less energy production in higher wind speeds near rated. So since parallel flows have increased TI and decreased wind speed and perpendicular flows decreased TI and increased wind speed, a hypothesis could be made that the changes of the noise barrier to the Turbulence Intensity could have a positive effect in energy yield. But this would require further investigation. Finally the impact of TI(%) in lifetime, fatigue, loading and O&M costs should be determined as well. As turbulence intensity might induce potential harmful excitations in the loading of the system and thus decrease lifetime and increase O&M costs.

4.2. Economic analysis and energy yield

Proper siting of turbines and local characteristics can affect greatly the energy yield. Even a slight change in the relative angle of the noise barrier with the local wind rose could have dramatic changes in the energy yield as seen in the results in Fig. 18. This is very relevant for noise barriers on curved road passages were the relative wind field rotation angle could vary significantly (such as seeing from top in Fig. 3). This is quite important for infrastructure designers who need to take decisions to install energy systems that are financially attractive.

Closing the economic loop in chapter 1, we evaluate the change of Levelized cost of electricity for a micro wind turbine on top of a noise barrier with respect to a reference case. It is presented in the equation below based on (Ragheb, 2017). We assume n = 20 years lifetime of the installed turbine and a discount rate i = 0.04. The reference LCOE is estimated including the I_t investment costs (or else CAPEX) and the O&M costs spent in year t. The investment costs I_t (€) is assumed in the order of 7000 €/kW installed. Annual O&M costs are assumed 1–2% of the CAPEX (Orrell and Poehlman, 2017). The AEP_o is the reference energy yield excluding the noise barrier.

$$LCOE_{reference}(h) = \frac{\sum_{t=1}^{n}(I_t + O\&M_t)\frac{1}{(1+i)^t}}{\sum_{t=1}^{n} AEP_0(h)} \tag{14}$$

Then we calculate LCOE of a turbine installed at 3 different heights h(m) and for various wind field rotations as used before. For the new LCOE we take into account the annual energy yield AEP_2 which includes the effect of the noise barrier of each height and wind field rotation. We assume a 20% cost reduction in the investments, due to exclusion of foundation and allocation of other costs of electrical infrastructure, installation, permitting, transportation, logistics and other costs as defined in (Orrell and Poehlman, 2017), and the findings of (Udell et al. 2010) with respect to lowering costs when retrofitting micro wind turbines on roofs.

$$LCOE(h,\delta) = \frac{\sum_{t=1}^{n}(I_t \cdot \kappa_{reduction} + O\&M_t)\frac{1}{(1+i)^t}}{\sum_{t=1}^{n} AEP_2(h,\delta)} \tag{15}$$

Finally we compare the reference with each calculated LCOE.

$$LCOE_{change} = \frac{LCOE(h,\delta)}{LCOE_{reference}(h)} \tag{16}$$

LCOE(€/kWh) decreases in most wind field rotation cases and different heights and is between 60 and 90% of the reference. Even though this is an overgeneralized interpretation it is a positive result meaning that with such a cost reduction and installation on a barrier we can expect higher energy yields and lower electricity costs. However, there are still cases in Fig. 19 where LCOE increases with a sensitive deviation such as between $\delta = 120^0$ and $\delta = 160^0$. Finally, the reference LCOE are 0.30€/kWh for 1.94H, 0.38€/kWh for 1.50H and 0.52€/kWh for 1.17H.

As presented in Fig. 19 LCOE could potentially decrease considerably but is very sensitive on the noise barrier relative angle to the wind rose (expressed in rotation angle $\delta(^0)$). This is quite positive for micro wind energy generation. However, we could potentially have 17.7 MW of micro wind energy generation on top of noise barriers in the Netherlands. This is quite a small number comparable to 6 wind turbines of ~3 MW, and is at a very low competitive level comparing to onshore wind prices of nearly 0.05 €/kWh (IRENA, 2019). This makes us conclude that viability of such projects is quite limited and further cost reduction is needed for example by using larger rotors along highways. However, micro wind energy is still an important part of wind energy developments where various applications may be powered.

5. Conclusions

Sonic anemometers were installed on top of a noise barrier and on a reference location to assess the effect of the noise barrier on the wind flow for all windward wind directions $\phi(^0)$. The properties of wind speed magnitude U(m/s), turbulence intensity TI(%) are assessed and compared. Additionally, the inflow angle $\theta(^0)$ is being assessed for its influence on the annual energy production AEP(kWh). A sensitivity assessment of the annual energy yield with a wind field rotation angle $\delta(^0)$ based on these results has been made for the application of a micro wind turbine installed on top of the noise barrier. Finally, the effect on the Levelized cost of electricity LCOE(€/kWh) is presented.

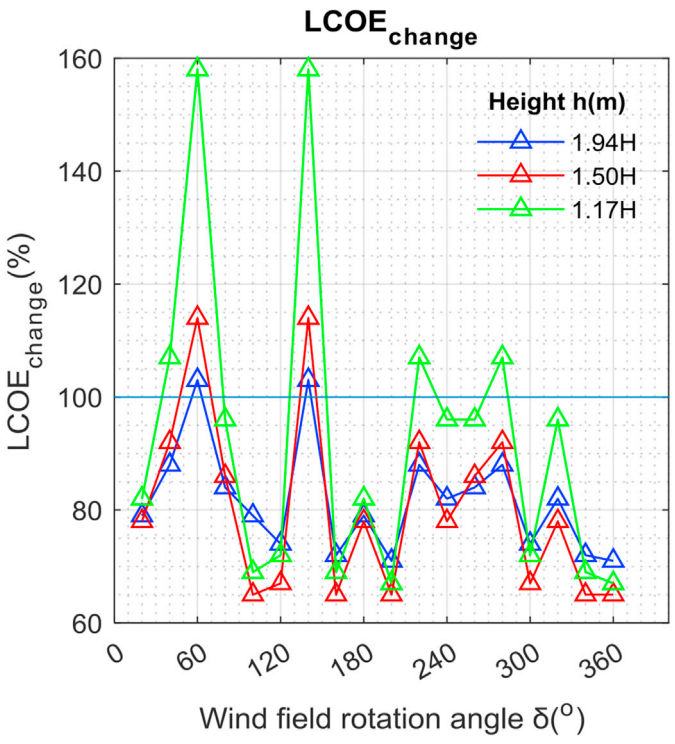

Fig. 19. LCOE change for different wind field rotation angles $\delta(^0)$ and heights h(m).

The most important findings are summarized in the following bullet points:

- Wind speed on top of noise barriers increases in perpendicular flows. The maximum increase of 36% is found at 1.19H and a 20% increase at 1.94H, with H representing the height of the barrier.
- Wind speed on top of noise barriers is decreasing in parallel flows with maximum decrease of 27% at 1.19H and 20% at 1.94H.
- Inflow angle is always skewed for all wind flow direction towards the barrier. The averages are in the range of 5^0 (at higher heights) to 25^0 (at lower height towards the barrier tip).
- Terrain and road network layout near a noise barrier affect the symmetry of changes that the barrier induces to approaching flows. Presence of a small bridge next to the barrier probably influences and shifts the local maxima of the changes, especially for wind speed and inflow angle.
- Turbulence intensity on top of a noise barrier for perpendicular flows (-30° until $+15^\circ$) drops with respect to the Reference Pole from 28%-40% to 22–32%. For parallel flows towards the barrier at ($+60^\circ$ until $+90^\circ$) the turbulence intensity range increases from 35-45% to 36–55%. For parallel flows (-60° until -90°) and ($+60^\circ$ until $+90^\circ$), it increases from 25%-35% to 25%–42%, with respect to the free-stream reference pole turbulence intensity ranges.
- Annual Energy yields could vary greatly even within 20° of wind field rotation from 110% down to 80% and back to 115% of the reference yield value. Installers are advised to perform wind resource assessment before installing.
- Effects on wind sped magnitude have the greatest contribution in the relative change in energy yield ranging from 60% to 150%. Skewed inflow angle losses should also be included as described before and range from 80% to 95% as a loss.
- Different combinations of height of installation and noise barrier (potential) orientation could bring variation in energy yield from 100 to 600 kWh for a 0.375 kW micro wind turbine
- Electricity cost reduction is possible for micro wind turbines on noise barriers due to the 20% investment cost reduction from structural integration and the energy yield increase due to the noise barrier flow effects. LCOE can drop to 60%–90% of the reference value. When we rotate the wind field annual time series in order to assess the sensitivity with respect to the noise barrier, we find that LCOE can dramatically change even in 20^0 increments of rotation. Finally, when comparing micro wind energy projects of the like with onshore wind energy we clearly see that micro wind is more expensive.

6. Recommendations-future studies

Based on results and all insight gained from the experiment and the data analysis process, we propose the following some of which will be part of the next series of publications of this project.

1) Micro-wind turbine installation on noise barrier to evaluate the behaviour and estimate the energy yield.
2) Wind tunnel testing to assess micro wind turbine's behaviour on misaligned flow conditions
3) Validation with more noise barrier sites and comparison with respect to surrounding roughness factors and zero-scale displacements and different year time series to assess the sensitivity
4) Measuring in more detail the influence of turbulence due to passing vehicles, as the examined noise barrier is placed on low speed limit road and other noise barriers are in higher speed limit.
5) Experimentation, modelling, analysis and correlation of the turbulent intensity effect of micro wind turbine yields on top of noise barriers
6) Wake flow studies from the dataset for all other flows
7) Validation of CFD studies of similar obstacles for urban flows or numerical simulations.
8) Other measurement techniques in order to capture detailed aspects of the relevant flows on top of the noise barrier (for example, smoke visualization, LiDar etc)
9) Experimental or modelling assessment of different turbine rotor sizes (pico/micro/small) and types, such as Vertical Axis Wind Turbines (VAWTs) or Diffuser-Augmenter Wind Turbines (DAWTs)
10) Discussion with local authorities for regulations regarding turbine installation next to highways.
11) Modelling of turbulence intensity impact on fatigue, loading, lifetime and O&M costs of the micro wind turbine integrated on top of a noise barrier.
12) Detailed economic analysis and survey with installation companies in order to identify installation, operation and maintenance costs of micro wind turbines integrated on noise barriers.
13) Wake losses in multiple turbines installation on noise barriers

Acknowledgements

The project is financed by STW (grant number-12728) under the acronym Duct4U. It involves design and implementation of ducted wind turbines on noise barriers. Partners specifically involved in the presented research are Windchallenge and Province of South Holland. Authors would like to acknowledge Sander van Vliet for facilitating and allowing of installations. Jeroen de Jong for all arrangements and installations. Municipality Pijnacker-Nootdorp for the special permits to conduct the experiments. Westland Infra and KD Telematica, who assisted in installation. DEMO workshop (TU Delft) for design of hardware, especially Daniel van Baarle. Nico van Beek, technical engineer at the OJF wind tunnel. Wittich and Visser who referred to TNO for the sonic anemometers. TNO for the sonic anemometers (specifically Erik Slis). Prof. Herman Russchenberg for providing DAVIS weather station. Last but very important all students who assisted into installation and data analysis Andrea Vilarasau Amoros (co-author), Miguel Rodríguez Escude, Michael Nash, Changzhi Liu and Yan Wang.

References

Abohela, I., Hamza, N., Dudek, S., 2013. Effect of roof shape, wind direction, building height and urban configuration on the energy yield and positioning of roof mounted wind turbines. Renew. Energy 50, 1106–1118. https://doi.org/10.1016/j.renene.2012.08.068.

Allen, S.R., Hammond, G.P., McManus, M.C., 2008. Energy analysis and environmental life cycle assessment of a micro-wind turbine. Proc. IME J. Power Energy 222, 669–684. https://doi.org/10.1243/09576509jpe538.

Bailey, B.H., McDonald, S.L., 1997. Wind Resource Assessment Handbook - Fundamentals of Conducting a Successful Monitoring Programme.

Balduzzi, F., Bianchini, A., Ferrari, L., 2012. Microeolic turbines in the built environment: influence of the installation site on the potential energy yield. Renew. Energy 45, 163–174. https://doi.org/10.1016/j.renene.2012.02.022.

Barthelmie, R.J., Pryor, S.C., 2018. The impact of wind direction yaw angle on cliff flows. Wind Energy 21, 1254–1265. https://doi.org/10.1002/we.2227.

Bastankhah, M., Porte-Agel, F., 2016. Experimental and theoretical study of wind turbine wakes in yawed conditions. J. Fluid Mech. 806, 506–541. https://doi.org/10.1017/jfm.2016.595.

Bowen, A.J., Lindley, D., 1977. A wind-tunnel investigation of the wind speed and turbulence characteristics close to the ground over various escarpment shapes. Boundary-Layer Meteorol. 12, 259–271. https://doi.org/10.1007/bf00121466.

Burton, T., Sharpe, D., Jenkins, N., Bossanyi, E., 2001. Wind Energy Handbook. John Wiley and Sons Ltd.

Changsoo, K., 2013. Sound Proof Wall Having Wind Power Generating Function. Korean Intellectual Property Office. Patent number: KR20130015568A.

Chen, G.H., Wang, W.W., Sun, C.F., Li, J.L., 2012. 3D numerical simulation of wind flow behind a new porous fence. Powder Technol. 230, 118–126. https://doi.org/10.1016/j.powtec.2012.07.017.

Chrysochoidis-Antsos, N., 2019. Sonic Anemometer Wind Speed Field for Urban Wind Flows Around a Noise Barrier (Acoustic Screen) and Weather Station Supplementary Dataset (Temperature, Wind, Solar). 4TU.Centre for Research Data. https://doi.org/10.4121/uuid:b878c00c-1c31-40bb-a3f4-0bed7aabb9ed. Dataset. *Grant number:* 12728 - Duct4U. *Funded by* STW.

Ciri, U., Rotea, M.A., Leonardi, S., 2018. Effect of the turbine scale on yaw control. Wind Energy 21, 1395–1405. https://doi.org/10.1002/we.2262.

Cochran, B., 2002. The influence of atmospheric turbulence on the kinetic energy available during small wind turbine power performance testing. Proceeding of IEA Expert meeting (CEDER-CIEMAT - Soria, Spain). Url: http://citeseerx.ist.psu.edu/viewdoc/download?doi=10.1.1.61.4472&rep=rep1&type=pdf.

Dierickx, W., Cornelis, W.M., Gabriels, D., 2003. Wind tunnel study on rough and smooth surface turbulent approach flow and on inclined windscreens. Biosyst. Eng. 86, 151–166. https://doi.org/10.1016/S1537-5110(03)00120-X.

Drew, D.R., Barlow, J.F., Cockerill, T.T., 2013. Estimating the potential yield of small wind turbines in urban areas: a case study for Greater London, UK. J. Wind Eng. Ind. Aerod. 115, 104–111. https://doi.org/10.1016/j.jweia.2013.01.007.

Eskridge, R.E., Rao, S.T., 1983. Measurement and prediction of traffic-induced turbulence and velocity-fields near roadways". J. Clim. Appl. Meteorol. 22, 1431–1443, 10.1175/1520-0450(1983)022<1431:Mapoti>2.0.Co;.

Encraft, 2009. Warwick wind trials report. Encraft. Url: http://www.microwindturbine.be/Rapportering_files/Warwick+Wind+Trials+Final+Report+%281%29.pdf.

Fu, R., Feldman, D., Margolis, R., Woodhouse, M., Ardan, K., 2017. U.S. Solar Photovoltaic System Cost Benchmark: Q1 2017. National Renewable Energy Laboratory (NREL). Url: https://www.nrel.gov/docs/fy17osti/68925.pdf.

Gi, S.C., 2009. Sound Proof Wall Having Wind Power Generating Function. Korean Intellectual Property Office. Patent number: KR100933575B1.

Gill Instruments. WindMaster and WindMaster PRO - user manual. Url: http://gillinstruments.com/data/manuals/windmaster-windmaster-pro-manual.pdf?iss=8.201512508.

Hagler, G.S.W., Tang, W., Freeman, M.J., Heist, D.K., Perry, S.G., Vette, A.F., 2011. Model evaluation of roadside barrier impact on near-road air pollution. Atmos. Environ. 45, 2522–2530. https://doi.org/10.1016/j.atmosenv.2011.02.030.

Heisler, G.M., Dewalle, D.R., 1988. Effects of windbreak structure on wind flow. Agric. Ecosyst. Environ. 22–3, 41–69. https://doi.org/10.1016/0167-8809(88)90007-2.

Honrubia, A., Vigueras-Rodriguez, A., Gomez-Lazaro, E., 2012. The influence of turbulence and vertical wind profile in wind turbine power curve. Progress in Turbulence and Wind Energy Iv 141, 251–254.

IEC, 2005. IEC 61400-12-1:2005(E) (Wind Turbines - Part 12-1: Power Performance Measurements of Electricity Producing Wind Turbines).

IRENA, 2019. Renewable Power Generation Costs in 2018. International Renewable Energy Agency. Url: https://www.irena.org/-/media/Files/IRENA/Agency/Publication/2019/May/IRENA_Renewable-Power-Generations-Costs-in-2018.pdf.

ISO, 2002. ISO 16622 - Meteorology - Sonic Anemometers/thermometers - Acceptance Test Methods for Mean Wind Measurements. International Organization for Standardization.

Kaiser, K., Langreder, W., Hohlen, H., Hojstrup, J., 2004. Turbulence Correction for Power Curves.

Kiwata, T., Nakata, H., Kuratani, T., Furumichi, H., Nakaguchi, A., Komatsu, N., 2011. Study of a performance of a cross-flow wind turbine located above a windbreak fence and the associated flow field. In: 21st National Symposium on Wind Engineering.

Kiya, M., Sasaki, K., 1983. Free-stream turbulence effects on a separation bubble. J. Wind Eng. Ind. Aerod. 14, 375–386.

KNMI, 2015. Rotterdam the hague AP (wind data) - station ID: 915096001". KNMI (koninklijk nederlands meteorologisch instituut). Url. https://wow.knmi.nl/.

Kosasih, B., Hudin, H.S., 2016. Influence of inflow turbulence intensity on the performance of bare and diffuser-augmented micro wind turbine model. Renew. Energy 87, 154–167. https://doi.org/10.1016/j.renene.2015.10.013.

Krynytzky, A., Ewald, B., 1998. AGARDograph 336 - Wind Tunnel Wall Corrections. North Atlantic Treaty Organization (NATO).

Largeau, J.F., Moriniere, V., 2007. Wall pressure fluctuations and topology in separated flows over a forward-facing step. Exp. Fluid 42, 21–40. https://doi.org/10.1007/s00348-006-0215-9.

Loganathan, B., Mustary, I., Chowdhury, H., Alam, F., 2017. Effect of turbulence on a Savonius type micro wind turbine. 1st International Conference on Energy and Power 110, 549–554. https://doi.org/10.1016/j.egypro.2017.03.183. Icep.2016.

Lubitz, W.D., White, B.R., 2007. Wind-tunnel and field investigation of the effect of local wind direction on speed-up over hills. J. Wind Eng. Ind. Aerod. 95, 639–661. https://doi.org/10.1016/j.jweia.2006.09.001.

Luo W., Lei X., and Z., Wang. "Wind Energy Utilization Type Load Reduction Sound Barrier". (2016). PRC) CNIPA (National Intellectual Property Administration. Patent number: CN106192786A.

Luo W., Lei X., and Z., Wang. "Wind Energy Utilization Type Subtracts a Year Sound Barrier". (2017). PRC) CNIPA (National Intellectual Property Administration. Patent number: CN206110000U.

Manwell, J.F., McGowan, J.G., Rogers, A.L., 2009. Wind Energy Explained - Theory, Design and Application. John Wiley & Sons Ltd.

Orrell, A.C., Poehlman, E.A., 2017. *Benchmarking U.S. Small wind costs"*. PNNL. Pacific northwest national laboratory. Url. https://wind.pnnl.gov/pdf/Benchmarking_US_Small_Wind_Costs_092817_PNNL.pdf.

Orrell, A., Foster, N., Morris, S., Homer, J., Preziuso, D., Pehlman, E., 2017. Distributed Wind Market Report. U.S. Department of Energy/Office of Energy Efficiency and Renewable Energy/Wind Energy Technologies Office, p. 2017. Url: https://www.energy.gov/sites/prod/files/2018/09/f55/2017-DWMR-091918-final.pdf.

Pena, A., Bechmannn, A., Conti, D., Angelou, N., 2016. The fence experiment - full-scale lidar-based shelter observations. Wind Energy Science 1, 101–114. https://doi.org/10.5194/wes-1-101-2016.

PZH, Province of South Holland. Miniwindturbine op geluidsscherm aan de N470 - Mini wind turbine on a noise barrier at N470 regional road". Published by: Province of South Holland. Released on: 26 April 2018, Url: https://www.zuid-holland.nl/onderwerpen/energie/energiewegen-0/n470-geeft-energie/@20807/miniwindturbine-n470/.

Ragheb, Magdi, 2017. Chapter 25 - economics of wind power generation. In: Letcher, Trevor M. (Ed.), Wind Energy Engineering. Academic Press, pp. 537–555.

Raine, J.K., 1974. Modelling the Natural Wind : Wind Protection by Fences. University of Canterbury (Christchurch)., *For the Doctoral degree*.

Rijkswaterstaat. GIS data for noise barriers and highways. Accessed on November 2018. Url: https://www.rijkswaterstaat.nl/kaarten/geluidregister.aspx?cookieload=true.

Rogers, T., Omer, S., 2012. Yaw analysis of a micro-scale horizontal-axis wind turbine operating in turbulent wind conditions. Int. J. Low Carbon Technol. 8, 58–63. https://doi.org/10.1093/ijlct/cts009.

Rowcroft, J., Burton, D., Blackburn, H.M., Sheridan, J., 2016. Siting wind turbines near cliffs - the effect of wind direction. Wind Energy 19, 1469–1484. https://doi.org/10.1002/we.2004.

Rowcroft, J., Burton, D., Blackburn, H.M., Sheridan, J., 2019. Siting wind turbines near cliffs: the effect of ruggedness. J. Fluid Eng.Trans. ASME 141. https://doi.org/10.1115/1.4041231, 031104-1.

Schreck, S.J., Schepers, J.G., 2014. Unconventional rotor power response to yaw error variations. J. Phys. Conf. 555, 012001 https://doi.org/10.1088/1742-6596/555/1/012001.

Schulz, C., Letzgus, P., Lutz, T., Kramer, E., 2017. CFD study on the impact of yawed inflow on loads, power and near wake of a generic wind turbine. Wind Energy 20, 253–268. https://doi.org/10.1002/we.2004.

Sunderland, K., Narayana, M., Putrus, G., Conlon, M., 2016. Levelised cost of energy analysis: a comparison of urban (micro) wind turbines and solar PV systems. In: 51st International Universities Power Engineering Conference (UPEC).

Tabrizi, A.B., Whale, J., Lyons, T., Urmee, T., 2015. Rooftop wind monitoring campaigns for small wind turbine applications: effect of sampling rate and averaging period. Renew. Energy 77, 320–330. https://doi.org/10.1016/j.renene.2014.12.037.

Udell, D., Infield, D., Watson, S., 2010. Low-cost mounting arrangements for building-integrated wind turbines. Wind Energy 13, 657–669. https://doi.org/10.1002/we.386.

van Bussel, G.J.W., Mertens, S.M., 2005. Small wind turbines for the built environment. In: 4th European & African Conference on Wind Engineering. Prague.

Wegley, H., Rammsdell, J., Orgill, M., Drake, R.L., 1980. A Siting Handbook for Small Wind Energy Conversion Systems. Pacific Northwest Laboratory.

WindLeaf. WindLeaf turbine specifications. Accessed on *February 2018*. Url: https://windchallenge.com/the-windleaf/#specs.

WMO, 2010. Guide to Meteorological Instruments and Methods of Observation. World Meteorological Organization. Url: https://library.wmo.int/pmb_ged/wmo_8_en-2012.pdf.

Woodruff, N.P., Read, R.A., Chepil W, S., 1959. Influence of a Field Windbreak on Summer Wind Movement and Air Temperatures.